Petroleum and Coal

IMPACT OF SMALL-SCALE HETEROGENEITY ON POTENTIAL RECOVERY IN SELECTED RESERVOIR SANDSTONES FROM WEST BARAM DELTA, OFFSHORE, SARAWAK

I. Yusuf, E. Padmanabhan

Department of Geosciences, Faculty of Geosciences and Petroleum Engineering, Universiti Teknologi PETRONAS, postcode 32610, Seri Iskandar, Perak, Malaysia

Abstract

Small-scale sedimentary heterogeneity in reservoir description is required for reliable recovery. West Baram Delta was selected as a case study because of the ongoing residual oil phase recovery in the area. This paper investigates effects of different small-scale sedimentary structures on permeability variation of selected reservoir sandstones using an integrated approach combining cores, thin sections, mercury injection capillary pressure data and tiny spot air permeameter. Two main sandstone lithofacies; namely massive fine grained and massive coarse grained sandstone lithofacies were identified to exhibit small-scale heterogeneity. The result indicates in massive fine grained sandstones characterized by fining-up grains with fossil shell fragments, *Ophiomorpha* burrows and faint lamination structures measured air permeability values along host sample accounted for 50% of varying air permeability from 79 mD to 648 mD and attributed to poor interconnectivity of pores resulting from grain packing and volume matrix content, as along coarse-fine boundary permeability varies between 249 mD to 1124 mD accounted for 50% permeability ascribed to variation in grain sorting and embedded shell fragments. Also along *Ophiomorpha* burrows, air permeability vary from 298 mD to 794 mD accounted for 45% permeability, but along host sediment permeability varies from 75 mD to 368 mD accounted for 55% increase. The measured permeability along lamina structure, values vary between 123 mD to 738 mD accounting for 55.6% also ascribed to grains topology that facilitates pore interconnectivity. But however, along host sediment air permeability varies from 89 mD to 448 mD accounted for 44.4% increase. In massive coarse grained sandstones characterized by faint lamination and biotubation, air permeability vary from 533 mD to 819 mD along lamina accounted for 60% and varies from 828 mD to 1188 mD along host sample, along biotubated spots permeability vary from 78 mD to 93 mD and is attributed to decrease in grain isotropy and sorting within region. It shows that the massive fine grained sandstones hold higher fluid flow potential advantage over massive coarse grained sandstone lithofacies in the delta. Furthermore, prior knowledge of small-scale sedimentary structure will give insight on potential recovery variations within different reservoir sandstone lithofacies as they either enhance or reduce permeability

Keywords: *Small-scale sedimentary heterogeneity; permeability variation; reservoir sandstone; pore diameter; oversize pores.*

1. Introduction

The measure of the ability of the rock to transmit fluids is known as permeability [1-2]. The goal of reservoir characterization is to generate models that allow the accurate prediction of future well performance and characterization of permeability heterogeneity to accurately understand flow behavior in reservoirs [3]. In petroleum reservoir modeling however, researchers acknowledge small-scale sedimentary structures plays an important role in oil recovery, perhaps incorporating knowledge of small-scale sedimentary heterogeneity in reservoir description is required for reliable prediction of oil production [3-6] for it significantly contributes to reservoir complexity. However, failure to adequately evaluate or take account of such variation and complexities in reservoir results in failure to optimize hydrocarbon production [6] in many fields. West Baram Delta is most prolific matured West Baram Delta field [7] is among

enlisted for an EOR process [7-9] to maximize oil production from some of the existing more than 170 production wells. This study is challenged to investigate the variable small – scale sedimentary structures in reservoir sandstone lithofacies that poses to impact fluid flow behavior of the reservoir. These because lateral continuity and connectivity of reservoir lithofacies are one of the high-ranking heterogeneities that are often ignored and difficult to predict [3] as they describe rock properties that potentially influence dynamic permeability measurement of the reservoir. In addition, permeability values obtained from outcrops are not very reliable [3], because they are not true representatives of reservoirs rock. This study is performed on cores from producing hydrocarbon reservoir to evaluate it dynamic permeability measurement. However, till date accurate estimation of permeability still remains challenge [10] in many fields.

2. Study area

The Baram Delta is mature field, and one of seven geological provinces, situated offshore, Sarawak, Malaysia (Figure 1). It is the most oil and gas prolific of all the geological provinces in the basin [11-12]. The oil-in-place in multiple stacked sandstone reservoirs were estimated to contain more than 0.48×108 m3 in a shallow offshore environment as at 1969 when the delta were discovered. More than eight fields have been found in Baram Delta, with more than 30 years production history, and presently with an average recovery factor of about 30% [12,27]. The offshore formations of the Baram Delta include coastal to coastal-fluviomarine sands deposited in a northwestward prograding delta since the Middle Miocene (from Cycle IV onwards), in which the Cycle V (Middle to Upper Miocene) to Cycle VII (Upper Pliocene) are the most developed [11-13]. Each cycle develops in a coastal plain envi-ronment to the south dominated by deposition of sands, silts and clays, and grades northwards into holomarine neritic to bathyal environments with deposition of mainly clays, silts, minor sands and, in places turbidities [14]. The sandstone core samples were taken from some wells in West Baram delta, which has obvious primary sedimentary heterogeneities feature in the form laminations, biotubation and cross-beddings which are apparently distinguishable from the several sandstone lithofacies [11,15] in the study area.
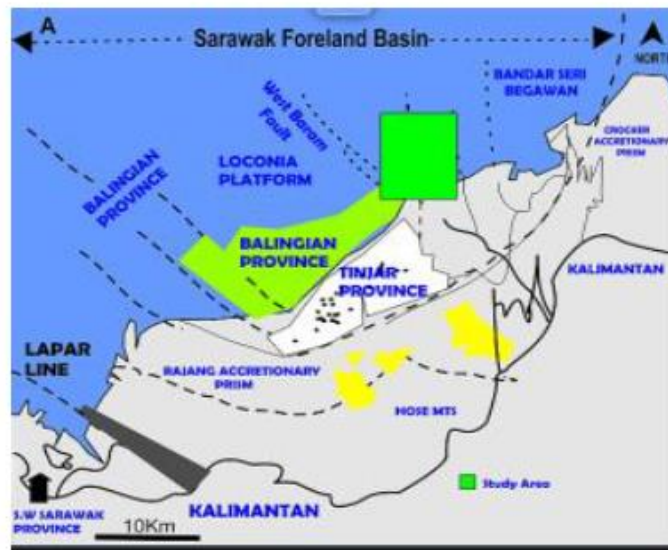

Figure 1. Location of the Sarawak basin and the study area

3. Materials and methods

The total of ninety-seven (97) core samples from exploratory wells within the Middle-Upper Miocene age within the Cycle IV and V lithological sequences were characterized into (5) five major lithofacies facies based on visible textural and sedimentary structures varying from

poorly stratified sandstone, low angle/parallel to crossed-bedding sandstone, biotubated sandstone. Tan [11] were identified and others reported are ripple cross - laminated sandstone, fining upward laminated, flaser bedded sandstones, massive coarse sandstone in the study area. Forty (40) sizeable hand core specimen samples, thin sections, mercury injection capillary pressure (MICP) and spot air-probe permeameter were integrated in this investigation.

The sandstone lithofacies and identification of sedimentary structures were carried out by conventional core logging with emphasis on texture and sedimentary structure [16-18]. The lithofacies description was complimented with thin section studies for pore sizes and textural composition analysis. Pore size was from measured using a scaled petrographic image analy-zer (JMicroVision 1.2.7), as obtained datasets in micrometers (μm) are converted to microns (μ) scale for matching the value ranges on mercury graphs generated from mercury injection capillary pressure (MICP). A gridded 1cm X 1cm line is drawn over the variable identified sedimentary heterogeneities on sandstone slab samples (Figure 2) as readings were taken at cross-spots (P). The 1cm X 1cm cube for air-probe permeability was measured using NER's Tiny Perm which is a portable hand-held air permeameter used for measurement of rock matrix permeability on outcrops and at the macro scale (3cm–3m). The permeability measurement range varies from approximately 10 millidarcys to 10 Darcys. The response function of the sample-instrument system is computed, and key characteristics of the response are displayed on the liquid crystal display (LCD). The results are then computed using the theoretical relation of the response function to permeability, the matrix permeability is determined from the calibration charts and tables provided with the instrument. In other to ensure the accuracy of the displayed measured values, reading was taken 4 -5 times at sample grid spot such the average was recorded before the conversion.

3.1. Petrography: Lithofacies description and pore sizes distribution

The faintly cross-stratified sandstone (Figure 2a) contains about 50.33 % coarse to medium grains, moderate to well sorted monocrystalline and polycrystalline quartz grains size ranging between 27-259μm with an average grain size of 104μm (Figure 3a). While matrix composition made up 30.25%, with an overall porosity of 19.42%. The variable measured pore sizes from thin section vary from 24931nm to 249980nm at an average of 96886nm constituted within overall porosity. This oversize pore [19] are indicated by low pressure region on the mercury bimodal (figure 4a) and will serve as a conduit for fluid flow [20]. Within the matrix filling intergranular space (see Figure 4a) measured pore size from thin section also vary from 1460nm to 39957nm at an average of 9083nm corresponding to the region of higher mercury pressure [20]. Furthermore, suggested inclusive within, are pores varying from 7.25nm – 99 nm ascribe altered to clay minerals and within 100nm to 1100 nm are ascribed to have resulted from dissolution pore cavities of feldspar mineral in the framework.

In the laminated, finning up sandstone with shell fragment sandstone lithofacies (Figure 2b), is a poorly sorted framework characterize by mottled structure appearance (Figure 3c & d). The grain size varies from 13.42μm to 139.3μm at an average value of 34.25μm having a total porosity of 7.67%. The embedded preserved fossil fragments during early deposition facili-tated visible intragranular pores (figure.3d). It also comprises predominantly monocrys-talline quartz grain and few polycrystalline grains at 24.58% proportion (Figure 3c & d) having 67.75% of matrix content.

The mercury unimodal graph shows pore size (figure 4c) correspond to measure shell cavities pores varying between 620 nm to 98992 nm with an average of 42080 nm. The unmarked pore sizes are resulting matrix within the range 6.25 nm–60 nm and 61nm–619nm all below thin section resolution.

In the cross stratified sandstone, biotubation with trace fossils (Figure 2c), grain size varies from 46.01μm to 262.2 μm with an average of 133.6 μm dominant monocrystalline quartz grain and few polycrystalline grains at 63.25%. It contains a matrix of 24.67% with a total porosity of 12.08% (Figure 3f). This lithofacies comprise of oversize pores [19] associated with changes in the energy of the depositional environment [21-22]. The measured pores from thin

section vary from 35286 nm to 112791nm at an average of 64895 nm correspond to the region of low pressure values in mercury bimodal (Figure 4e).
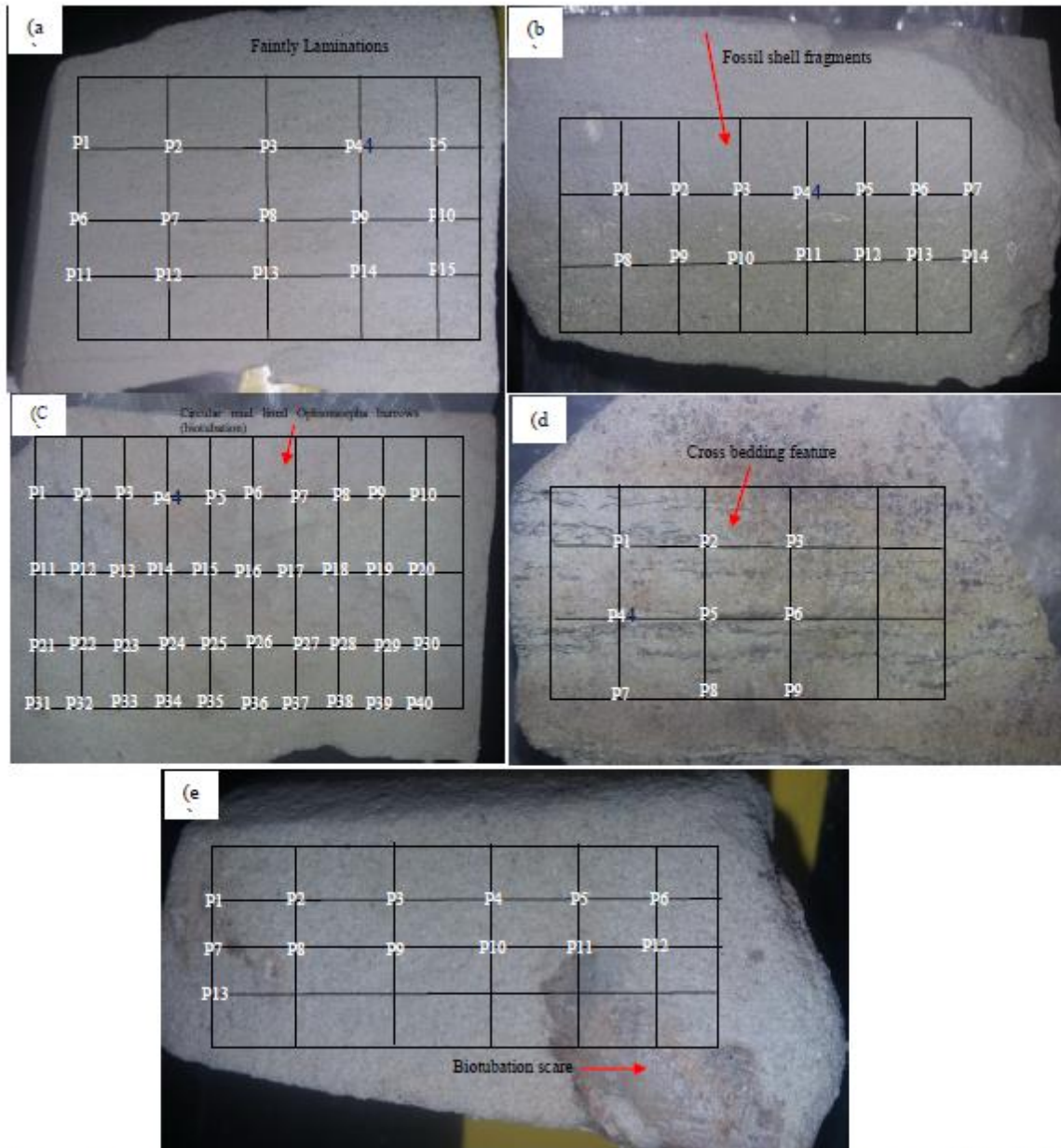
Figure 2. Showing variable sedimentary structures (a) Faintly cross-stratified sandstone with no trace fossils (b) laminated, finning up sandstone with shell fragments (c) cross stratified sandstone, circular mud lined Ophiomorpha burrows (biotubation) presence of high content of iron oxides and clay (d) cross laminated sandstone with no biotubation features (e) coarse biotubation sandstone lithofacies

The sedimentary cross laminated structured sandstone lithofacies (Figure 2d) has a porosity of about 4.08% with matrix content of 50.08% composition. The monocrystalline grain size varies from 67.7µm to 316.6µm averaging to 172.7µm, but little polycrystalline quartz totaling to 45.83% (Fig 3g) composition. The developed oversize (Fig. 3h) measured from microphotographs pore vary from 42238 nm to 135635 nm at an overall average of 74151 nm as indicated in mercury bimodal (Figure 4d)
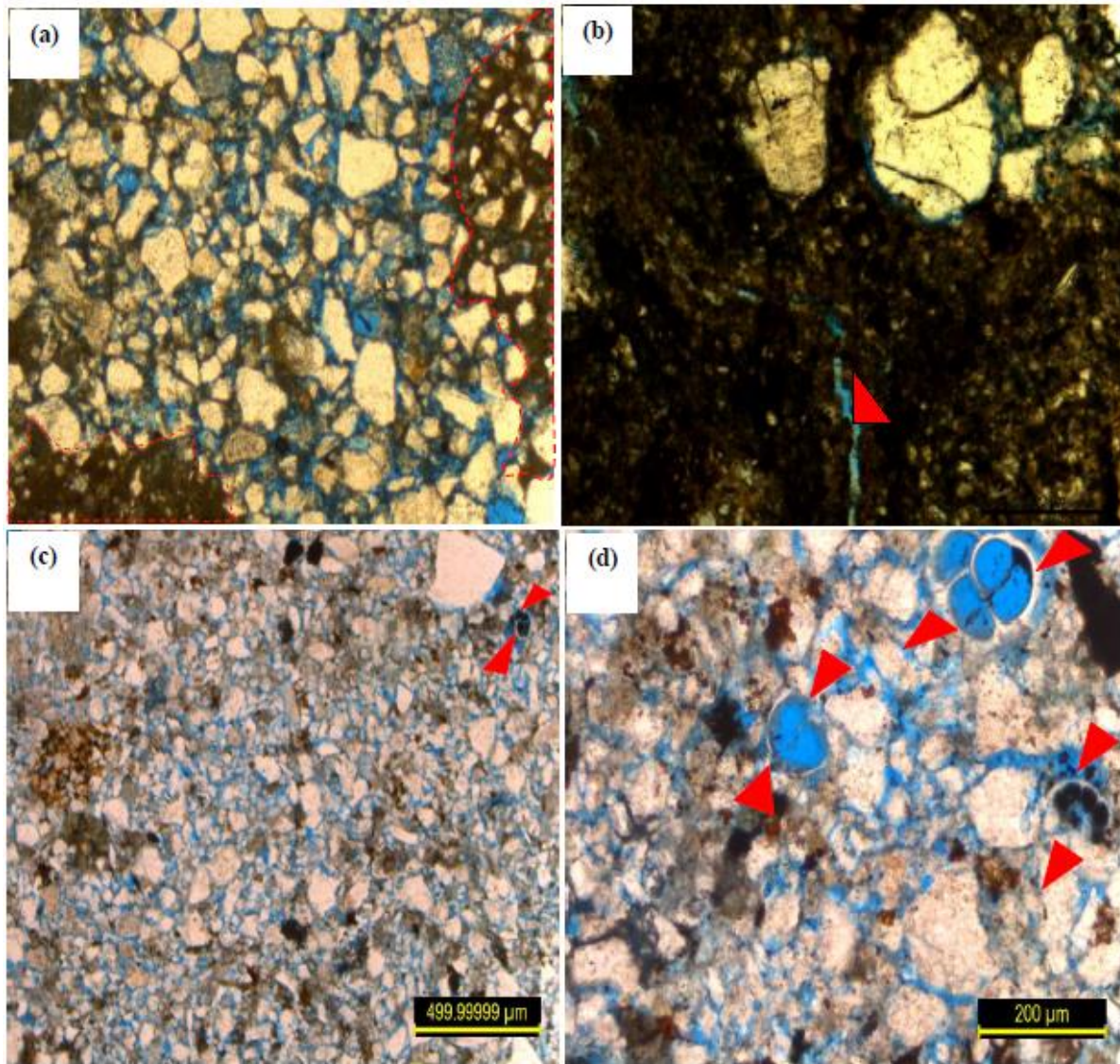
Figure 3. Showing thin section (A) faintly cross-stratified sandstone with random matrix filling (indicated with red dotted line) and (B) pore space within matrix indicated with red arrow (C) laminated, finning up sandstone with shell fragment facies (D) indicating intra pores within shell fragment cavities depict with red arrows

The coarse biotubation sandstone lithofacies (figure 2e), is texturally matured with moderately to well-sorted grain. It comprises of 44.17% monocrystalline and polycrystalline quartz grains. The sub-matured sandstone is having loosely (figure 3e) intergranular oversize pores [19] totaling to 11.05% porosity, and a matrix of 44.33%. The measured pore sizes from a thin section within it matrix (as depicted in figure 3a) varying from 168 nm to 119656 nm with an average of 18749 nm and 91319 nm are intergranular pores as indicated in mercury bimodal (see Figure 4e).
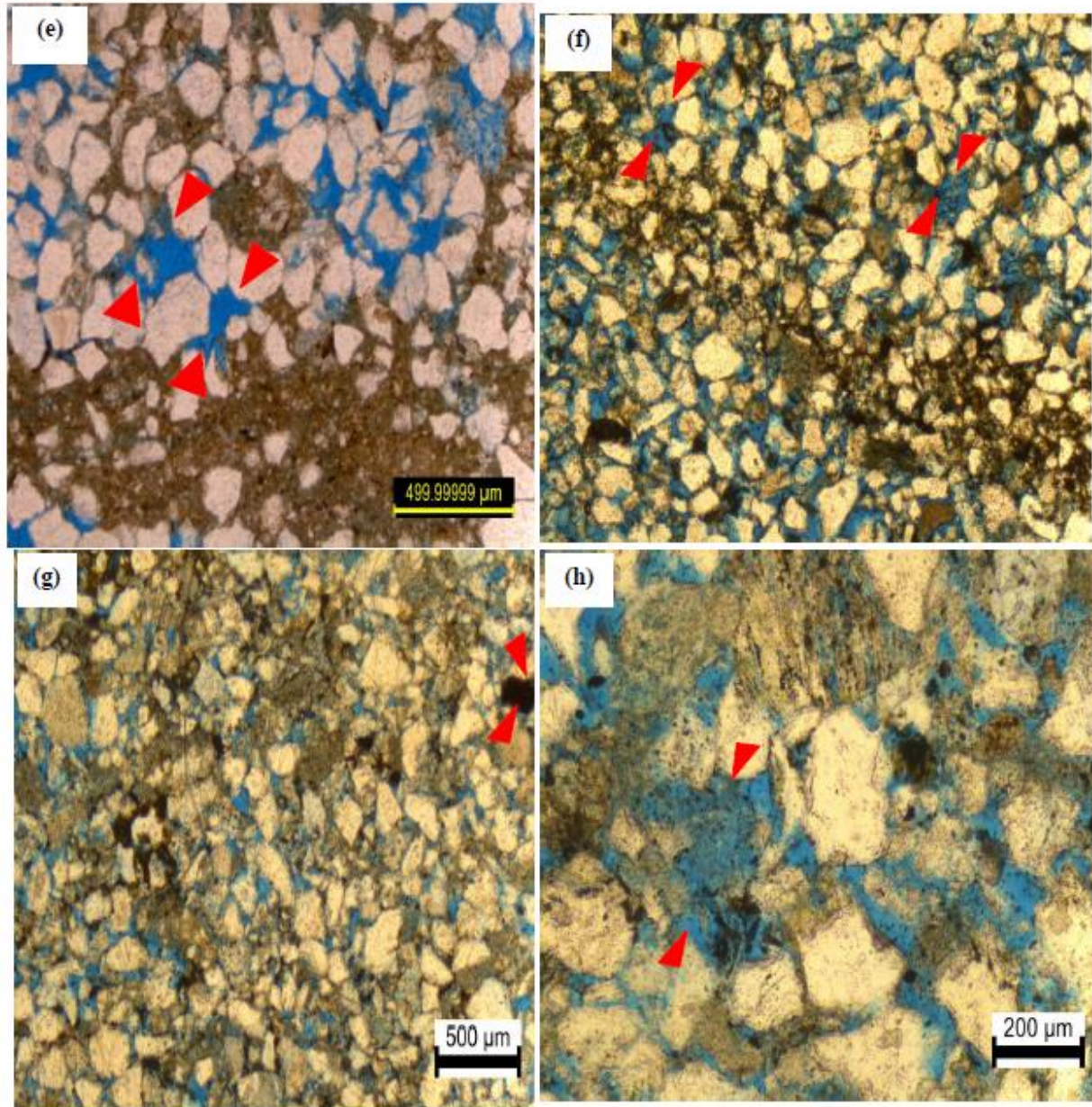
Figure 4 (e). Matrix in fill and oversize pores indicated with red arrows (f) pore cross stratified sandstone, biotubated sandstone facies indicated by red arrow (g) cross laminated sandstone facies with oversize pore indicated (h) with red arrows

4. Results and discussion

4.1. Impact of small-scale heterogeneities on permeability variations

The variable internal textural compositional suites and distributions in faintly cross stratified, laminated fining up, cross laminated and cross stratified with circular mud line *Ophiomorpha burrows* sedimentary structured sandstone lithofacies excluding coarse biotubated lithofacies suggest to contain both coarse-and fine foreset laminae [23-24].

These inhomogeneous internal configuration, differences in origins and distribution of pore types (Figure a; c; e; g & i) reveal to have different effects on permeability measurement [25-26]

at every crossed-points (P1-Pn) on gridded variable sedimentary structure, Figure 2a – e presented in Figure 4(b; d; f, h & j) and Table 1-5.
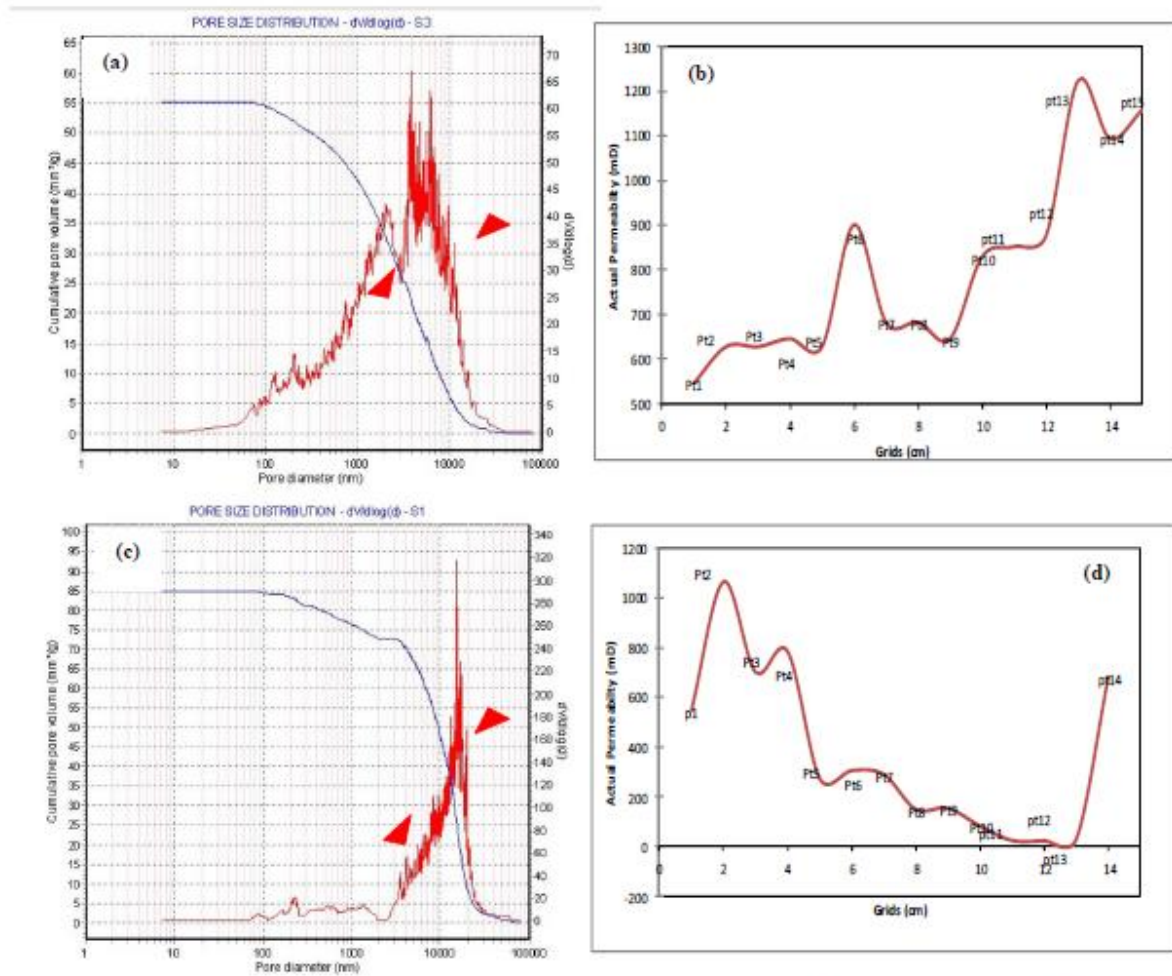

Figure 5 (a). Showing corresponding pore sizes in mercury bimodal (nm) indicated with red arrows (b) impact of small-scale heterogeneity at point spots on permeability in cross-stratified sandstone (c) corresponding pore sizes in mercury bimodal (nm) indicated with red arrows (d) impact of small - scale heterogeneity at point spots on permeability in laminated, finning up sandstone lithofacies

Table 1. Permeability distribution in the faintly laminated cross stratified sandstone lithofacies

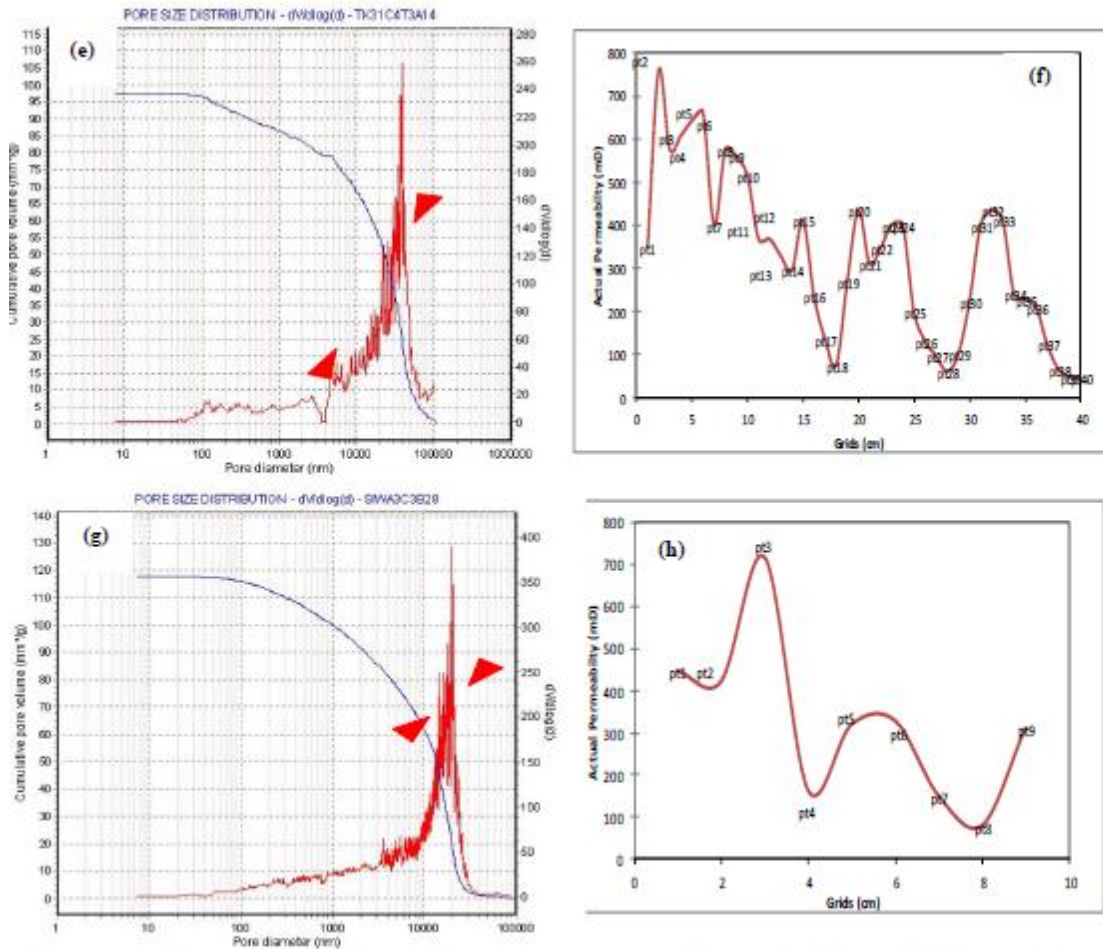| Point number	Permeability 10^{-3} µm²	Point description	Point number	Permeability 10^{-3} µm²	Point description
P1	533	Lamina structure	P9	618	Lamina structure
P2	635	Lamina structure	P10	819	Lamina structure
P3	628	Lamina structure	P11	828	Host sample
P4	618	Lamina structure	P12	910	Host sample
P5	592	Lamina structure	P13	1188	Host sample
P6	893	Host sediment	P14	1120	Host sample
P7	682	Lamina structure	P15	1140	Host sample
P8	693	Lamina structure			

Figure 5 (e). Showing corresponding pore sizes in mercury bimodal (nm) indicated with red arrows (f) impact of small-scale heterogeneity at point spots on permeability in cross laminated sandstone (g) corresponding pore sizes in mercury bimodal (nm) indicated with red arrows (h) impact of small - scale heterogeneity at point spots on permeability in coarse biotubated sandstone lithofacies

Table 2. Permeability distribution in laminated, finning up sandstone with shell fragment lithofacies

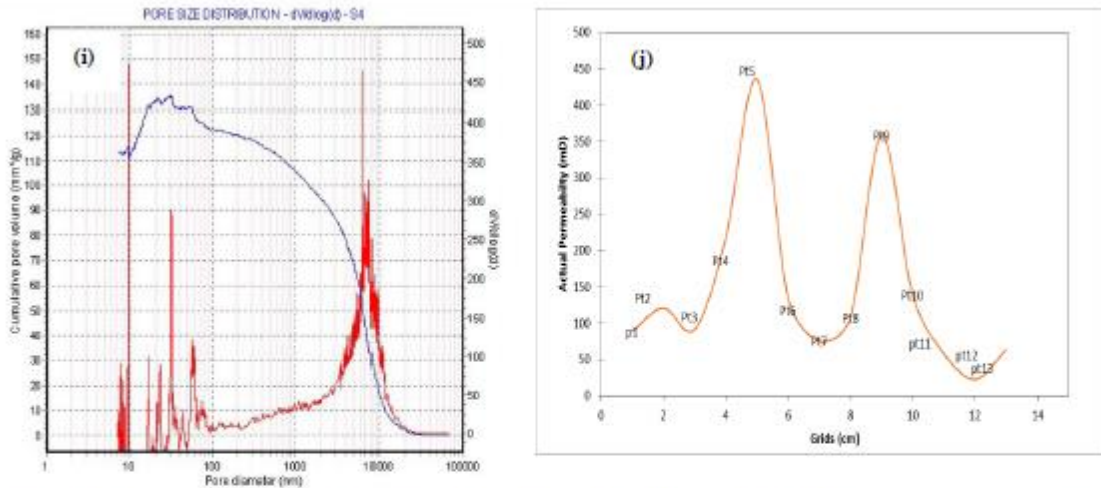| Point number	Permeability/10^{-3} μm^2	Point description
P1	498	Host sample (fining section)
P2	1124	Host sample (boundary between coarse -fining section)
P3	726	Host sample (boundary between coarse -fining section)
P4	793	Host sample (boundary between coarse -fining section)
P5	253	Host sample (boundary between coarse -fining section)
P6	234	Host sample (boundary between coarse -fining section)
P7	249	Host sample (boundary between coarse -fining section)
P8	168	Host sample (coarsening up section)
P9	171	Host sample (coarsening up section)
P10	121	Host sample (coarsening up section)
P11	118	Host sample (coarsening up section) with fossil
P12	98	Host sample (coarsening up section)
P13	79	Host sample (coarsening up section)
P14	648	Host sample (coarsening up section)

Figure 5 (i). Showing corresponding pore sizes in mercury bimodal (nm) indicated with red arrows (j) impact of small- scale heterogeneity at point spots on permeability in cross laminated sandstone

Table 3. Permeability distribution in cross stratified sandstone, *circular mud lined Ophiomorpha burrows* (biotubation) lithofacies

Point number	Permeability 10^{-3} μm^2	Point description	Point number	Permeability 10^{-3} μm^2	Point description
P1	348	Ophiomorpha burrows scare	P21	301	Host sediment
P2	794	Ophiomorpha burrows scare	P22	368	Host sediment
P3	598	Ophiomorpha burrows scare	P23	398	Ophiomorpha burrows scare
P4	564	Ophiomorpha burrows scare	P24	378	Ophiomorpha burrows scare
P5	645	Ophiomorpha burrows scare	P25	179	Host sediment
P6	631	Ophiomorpha burrows scare	P26	144	Host sediment
P7	398	Host sediment	P27	186	Ophiomorpha burrows scare
P8	567	Ophiomorpha burrows scare	P28	73	Host sediment
P9	558	Ophiomorpha burrows scare	P29	118	Host sediment
P10	512	Host sediment	P30	219	Host sediment
P11	355	Host sediment	P31	368	Ophiomorpha burrows scare
P12	410	Ophiomorpha burrows scare	P32	411	Ophiomorpha burrows scare
P13	310	Host sediment	P33	352	Host sediment
P14	298	Ophiomorpha burrows scare	P34	216	Host sediment
P15	416	Ophiomorpha burrows scare	P35	218	Ophiomorpha burrows scare
P16	242	Host sediment	P36	197	Host sediment
P17	143	Host sediment	P37	112	Host sediment
P18	75	Host sediment	P38	87	Host sediment
P19	268	Host sediment	P39	82	Host sediment
P20	448	Ophiomorpha burrows scare	P40	51	Host sediment

Table 4. Permeability distribution in cross bedding sandstone lithofacies

Point number	Permeability 10^{-3} μm^2	Point description
P1	448	Host sediment
P2	398	Host sediment (lamina structure)
P3	738	Host sediment (lamina structure)
P4	128	Host sediment (lamina structure)
P5	309	Host sediment
P6	298	Host sediment (lamina structure)
P7	123	Lamina structure
P8	89	Host sediment
P9	300	Host sediment

Table 5. Permeability distribution in coarse biotubation sandstone lithofacies

Point number	Permeability 10^{-3} μm²	Point description
P1	93	Host sediment (biotubated scare)
P2	128	Host sediment
P3	89	Host sediment (biotubated scare)
P4	189	Host sediment
P5	438	Host sediment
P6	113	Host sediment
P7	78	Host sediment (biotubated scare)
P8	111	Host sediment
P9	370	Host sediment
P10	119	Host sediment
P11	76	Host sediment (biotubated scare)
P12	48	Host sediment (biotubated scare)
P13	52	Host sediment (biotubated scare)

However, biotubation either enhances permeability due to a different degree of burrowing activity and burrow fillings or perhaps reduces permeability [12] because of grain reworking and resorting. However, in faintly cross-stratified sandstone the consequential increase per-meability values (see Figure 2a) suggest due to oversize pores in fabric framework (see Figure 3a & b) as it reveals measured average pore diameter to vary from 9083 nm to 96886 nm marked in mercury injection graph. In the laminated, finning up sandstone with shell fragments sandstone facies (figure 2b), have a porosity of 7.67%. The measured intrapores preserved within the framework by variable shell cavity sizes at an average of 42080 nm embedded grandmas matrix of 67.75%. These, however, suggest responsible for the increase in permea-bility values at some cross-points (figure 4d), while decrease at some cross-points are attributed to the impact of coarse - and fine foreset [23-24] composition varying pore sizes.

Furthermore, in the cross stratified sandstone, *circular mud lined Ophiomorpha burrows* (biotubation); Figure 2c, the variability in permeability value are attributed the discrete coarse-fine grains making up the 12.08% total porosity. The measured pore diameters from thin section average at 64895 nm indicated also in mercury bimodal (figure 4e) by a decrease in pressure [25]. The variation in permeability values (figure 4h) in the cross laminated sand-stone with no biotubation features (figure 2d) having a low porosity of 4.08% (Figure 3g). The measured pore size diameter (Figure 3h) from thin section average at 74151 nm as indicated in mercury bimodal (Figure 4g). In coarse biotubation sandstone (figure 2e), having matrix content of 44.33% composing intergranular oversize [19] pore diameter at an average of 913159 nm amounting to 11.05% porosity as indicated in mercury bimodal (Figure 4i). However, measured intra pore diameters within the matrix in fill (see figure 3b) vary from 168 nm to 119656 nm suggest variations in permeability values at the cross points in figure 4j.

5. Conclusion

The result concluded that small - scale sedimentary heterogeneities have a potential impact on permeability [3-6] variation in all studied sandstone lithofacies as indicated in spot air permeameter values. These variabilities are attributed to the internal textural compositional suites and distributions containing both coarse - and fine foreset laminae [21,23-24], as biotubation also either enhances permeability due variable degree of burrowing activity and burrow fillings or perhaps reduces permeability [12] because of grain re-sorting. The inhomogeneity in the internal configuration resulting from the pattern visible primary structures contribute to having variable effects on pore sizes distribution, fluid flow unit [3] and permeability measurement [25-26] at every crossed-points (P1- Pn) on the gridded variable sedimentary structure in studied sandstone lithofacies. Thus, acknowledging and understanding the variable effect of small – scale sedimentary heterogeneities at macroscale

(3cm – 3m's thick) would be useful as requirements for reliable prediction of fluid flow in hydrocarbon production and oil recovery during reservoir modeling.

Acknowledgment

References

[1]   Tiab D and Donaldson EC. Petrophysics: theory and practice of measuring reservoir rock and fluid transport properties. Gulf Professional Publishing, 2015.

[2]   Ben-Awuah J and Padmanabhan E. Porosity and Permeability Modifications by Diagenetic Processes in Fossiliferous Sandstones of the West Baram Delta., Offshore Sarawak, 2014.

[3]   Mikes D. Sampling procedure for small-scale heterogeneities (crossbedding) for reservoir modelling. Marine and Petroleum Geology, 2006; 23: 961-977.

[4]   Morton K, Thomas S, Corbett P and Davies D. Detailed analysis of probe permeameter and interval pressure transient test permeability measurements in a heterogeneous reservoir. Petroleum Geoscience, 2002; 8: 209-216.

[5]   Willis BJ and White CD. Quantitative outcrop data for flow simulation. Journal of Sedimentary Research, 2000; 70: 788-802.

[6]   Huysmans M, Peeters L, Moermans G and Dassargues A. Relating small-scale sedimentary structures and permeability in a cross-bedded aquifer. Journal of Hydrology, 2008; 361: 41-51.

[7]   Latief AI, Ridzuan AI, Faehrmann PA, MacDonald AC, Arina W and Rahman G. An Innovative Static Modeling Approach to handle a Complex Giant within a Compressed Timeframe; A Case Study of Baram Oil Field, Offshore Sarawak, East Malaysia. in SPE Asia Pacific Oil and Gas Conference and Exhibition, 2012.

[8]   Khatib H. IEA world energy outlook 2011—A comment. Energy policy. 2012; 4: 737-743.

[9]   Abdullah R. Oil & Gas Industry–Opportunities and Challenges Ahead. Retrieved on February. 2012; 3: 47-61.

[10]   Ben-Awuah J and Padmanabhan E. An enhanced approach to predict permeability in reservoir sandstones using artificial neural networks (ANN). Arabian Journal of Geosciences, 2017; 10: 173-183.

[11]   Tan D, Rahman A, Anuar A, Bait B, and Tho CK. West Baram Delta. The Petroleum Geology and Resources of Malaysia, Petroliam Nasional Berhad (PETRONAS), Kuala Lumpur, 1999. 291-341.

[12]   Ben-Awuah J and Eswaran P. Effect of bioturbation on reservoir rock quality of sandstones: A case from the Baram Delta, Offshore Sarawak, Malaysia. Petroleum Exploration and Development, 2015; 42: 223-231.

[13]   Hutchinson Jr C, Dodge C and Polasek T. Identification, classification and prediction of reservoir nonuniformities affecting production operations. Journal of Petroleum Technology, 1961; 13: 223-230.

[14]   Rijks E. Baram Delta geology and hydrocarbon occurrence. Geol. Soc. Malays. Bull, 1981; 14: 1-8.

[15]   Abdulrahman AH, Menier D, and Mansor YM. Sequence stratigraphy modeling and reservoir Architecture of the shallow marine succession of Baram Field, West Baram Delta offshore Sarawak, East Malaysia. Mar. and Petrol. Geol., 2014; 4: 687-703.

[16]   Pettijohn F, Potter P, and Siever R. Sand and Sandstone. New York/Heidelberg/Berlin, 1973.

[17]   Tucker ME. Sedimentary rocks in the field. John Wiley & Sons, 2003.

[18]   Boggs S. Petrology of sedimentary rocks. Cambridge University Press, 2009.

[19]   James RA. Application of petrographic image analysis to the characterization of fluid-flow pathways in a highly-cemented reservoir: Kane Field, Pennsylvania, USA. Journal of Petroleum Science and Engineering, 1995; 13: 141-154.

[20]   Ehrlich R, Prince C, and Carr MB. Sandstone reservoir assessment and production is fundamentally affected by properties of a characteristic porous microfabric. in SPE Annual Technical Conference and Exhibition, 1997.

[21]   Evans RC. An investigation into the influence of common sedimentary structures and diagenesis on permeability heterogeneity and anisotropy in selected sands and sandstones. 1987.

[22]   Martinius AW, Howell J, Steel R, and Wonham J. From Depositional Systems to Sedimentary Successions on the Norwegian Continental Margin (Special Publication 46 of the IAS): John Wiley & Sons, 2014.

[23]   Hurst A, and Rosvoll KJ. Permeability variations in sandstones and their relationship to sedimentary structures. in Reservoir Characterization II, ed: Elsevier, 1991: 166-196.

[24]   Hartkamp-Bakker CA. Permeability heterogeneity in cross-bedded sandstones: impact on water/oil displacement in fluvial reservoirs. TU Delft, Delft University of Technology, 1993.

[25]   McCreesh CA, Ehrlich R, and Crabtree SJ. Petrography and Reservoir Physics II: Relating Thin Section Porosity to Capillary Pressure, the Association Between Pore Types and Throat Size (1). AAPG Bulletin, 1991; 75: 1563-1578.

[26]   Passey QR, Bohacs K, Esch WL, Klimentidis R, and Sinha S. From oil-prone source rock to gas-producing shale reservoir-geologic and petrophysical characterization of unconventional shale gas reservoirs. in International Oil and Gas Conference and Exhibition in China, 2010.

[27]   Abu Bakar M, Chong YY, Nasir E, Din A, Chai CF, Fui CC, Agarwal B, Valdez R, Adamson GR. EOR Evaluation for Baram Delta Operations Fields, Malaysia. in *SPE* Enhanced Oil Recovery Conference, Indonesia 2011, SPE 144533.

To whom correspondence should be addressed: I. Yusuf, Department of Geosciences, Faculty of Geosciences and Petroleum Engineering, Universiti Teknologi PETRONAS, postcode 32610, Seri Iskandar, Perak, Malaysia